# Multiphase Lattice Boltzmann simulations of droplets in microchannel networks

La Houille Blanche, n° 5, 2013, p. 5-11 DOI 10.1051/lhb/2013037

# Multiphase Lattice Boltzmann simulations of droplets in Microchannel networks

Jonathan LI[1], Yonghao ZHANG[1], Jason M REESE[2]

[1.] *James Weir Fluids Laboratory, Department of Mechanical & Aerospace Engineering, University of Strathclyde, Glasgow, G1 1 XJ, UK, jonathan.li@strath.ac.uk, yonghao.zhang@strath.ac.uk*

[2.] *School of Engineering, University of Edinburgh, Edinburgh, EH9 3JT, jason.reese@strath.ac.uk*

ABSTRACT. – In this work we study droplet flows in three different microchannel networks by using a multiphase lattice Boltzmann method. It is firstly shown that the lattice Boltzmann method is suitable for simulating droplet flows in complex microchannel geometries. The effect of velocity in the channels downstream of a branching intersection on the path a droplet would take through a microchannel network is investigated. We find that, for the investigated microchannel geometries, droplets that reached a channel intersection would travel through the downstream branch with the highest local velocity.

Key-words: microdroplets, microfluidics, lattice Boltzmann method, microchannel networks, multiphase flow

## Simulations par Boltzmann sur réseau multiphasique de gouttelettes dans des réseaux de microcanaux

RÉSUMÉ. – Dans ce travail, nous étudions les écoulements de gouttelettes dans trois réseaux différents de microcanaux en utilisant une méthode de Boltzmann sur réseau multiphasique. Il est tout d'abord montré que la méthode est adaptée pour simuler les écoulements de gouttelettes dans des microcanaux à géométries complexes. L'effet de la vitesse dans les canaux en aval d'une intersection sur le trajet pris par une gouttelette traversant un réseau de microcanaux est étudié. Nous constatons que, pour les géométries de microcanaux étudiés, les gouttelettes qui atteignent une intersection traverseraient la branche aval où la vitesse locale est la plus élevée.

Mots-clés : microgouttes, microfluidique, Boltzmann sur réseau, réseau de microcanaux, multiphasique

## I. INTRODUCTION

In recent years, droplet-based microfluidic devices have attracted significant interest within the biology and chemistry communities due to their huge potential for cost and time savings, enhanced analysis sensitivities, and accuracy. Useful applications include polymerase chain reaction [Mohr *et al.*, 2007], microfluidic logic gates [Cheow *et al.*, 2007], droplet reactors and uniform emulsions [Stone *et al.*, 2004]. However, a deeper understanding of droplet dynamics in microchannels is still necessary to fully exploit this potential. The predominant design methodology for microdroplet device design is currently trial and error, which is costly and time consuming. Insights to droplet behaviour would allow more rational design methodologies to be developed.

Many experimental studies have been carried out to develop understanding of droplet behaviour within microchannels. Many of them have been focused on passive droplet formation within microfluidic T-junctions and flow focusing geometries [Christopher *et al.*, 2008, Garstecki *et al.*, 2006, Xu *et al.*, 2006]. In the last few years, however, research has been focused on studying the behaviour of droplets in more complicated microchannel geometries [Choi *et al.*, 2011, Glawdel *et al.*, 2011, Parthiban, Khan, 2012].

Compared to experimental work, there have been significantly fewer computational studies into droplet behaviour. Such studies are important for obtaining detailed information that is difficult to experimentally measure. The lattice Boltzmann method is a candidate that can be used to simulate microdroplet flows. Although many lattice Boltzmann microdroplet simulations for simple microchannel geometries such as T-junctions and cross-junctions [Gupta, Kumar, 2010, Liu, Zhang, 2011, van der Graaf *et al.*, 2006] have been reported, little has been done for more complex microchannel networks.

In this paper, we study the flow of droplets in three different microchannel networks using the colour-fluid lattice Boltzmann method.

## II. LATTICE BOLTZMANN METHOD

The lattice Boltzmann (LB) equation can be expressed as [Chen, Doolen, 1998]

$$f_i(x + e_i\delta t, t + \delta t) - f_i(x, t) = \Omega_i \tag{1}$$

where $f_i$, $e_i$ and $\Omega_i$ are respectively the particle distribution function, discrete velocity and collision operator in the $i$th direction at position $x$ and time $t$ and $\delta t$ is the discrete time step. The most commonly used collision operator is the single relaxation time BGK collision operator [Qian *et al.*, 1992]

$$\Omega_i = -\frac{1}{\tau}\left(f_i(x,t) - f_i^{eq}(x,t)\right), \tag{2}$$

where $\tau$ is the relaxation time, $f_i^{eq}$ is the particle equilibrium distribution function, which is defined as

$$f_i^{eq} = \rho(x,t)\omega_i\left[1+\frac{e_i\cdot u(x,t)}{c_s^2}+\frac{1}{2}\frac{\left(e_i\cdot u(x,t)\right)^2}{c_s^4}-\frac{1}{2}\frac{u^2(x,t)}{c_s^2}\right], \quad (3)$$

where $\rho$ and $u$ are the local density and velocity, $\omega_i$ is the weight factor in the $i$th direction and $c_s$ is the lattice sound speed which is $c_s = c/\sqrt{3}$, where $c = \delta x/\delta t$, with $\delta x$ being the lattice spacing. The density and velocity at each lattice node can be calculated using

$$\rho(x,t) = \sum_i f_i(x,t), \quad (4)$$

$$u(x,t) = \frac{1}{\rho}\sum_i f_i(x,t)e_i, \quad (5)$$

and the kinematic viscosity is related to the relaxation time by

$$\nu = \frac{c_s^2}{\delta t}\left(\tau-\frac{1}{2}\right). \quad (6)$$

To simulate droplets, we use the colour-fluid multiphase LB model reported by Liu and Zhang [Liu, Zhang, 2011], which, compared to the original model of [Gunstensen *et al.* 1991], benefits from very low interfacial currents and greatly reduced lattice pinning tendencies. The colour-fluid lattice Boltzmann model introduces two particle distribution functions $r_i$ and $b_i$ to represent "red" and "blue" fluids. The particle distribution function $f_i$ is defined as

$$f_i(x,t) = r_i(x,t) + b_i(x,t) \quad (7)$$

and the local density of the red and blue fluids at each node is

$$\rho_R(x,t) = \sum_i r_i(x,t), \quad (8)$$

$$\rho_B(x,t) = \sum_i b_i(x,t). \quad (9)$$

To account for interfacial effects, the forcing term

$$\phi_i(x,t) = \frac{\omega_i}{c_s^2}e_i\cdot F(x,t), \quad (10)$$

where $F$ is the interfacial force, is introduced into the LB equation, which becomes

$$f_i(x+e_i\delta t, t+\delta t) - f_i(x,t) = -\frac{1}{\tau(x,t)}\left(f_i(x,t)-f_i^{eq}(x,t)\right)+\phi_i(x,t). \quad (11)$$

To account for the different viscosities of both fluids the relaxation time at each node is defined as

$$\tau(x,t) = \frac{\rho_R(x,t)}{\rho(x,t)}\tau_R + \frac{\rho_B(x,t)}{\rho(x,t)}\tau_B, \quad (12)$$

where $\tau_R$ and $\tau_B$ are respectively the relaxation times for the red and blue fluid.

The continuum surface force approach [Brackbill *et al.*, 1992] proposed by [Lishchuk *et al.*, 2003] is used at the fluid interfaces to model the interfacial tension between the fluids, with the force defined as

$$F(x,t) = -\frac{1}{2}\sigma K\nabla\rho^N, \quad (13)$$

where $\sigma$ is the interfacial tension, K is the curvature and $\rho^N$ is a phase field parameter, defined as

$$\rho^N(x,t) = \frac{\rho_R(x,t)-\rho_B(x,t)}{\rho(x,t)}. \quad (14)$$

The curvature can be calculated as

$$K = -\nabla_s\cdot n, \quad (15)$$

where the surface differential operator $\nabla_s$ is defined as

$$\nabla_s = (I - n\otimes n)\cdot\nabla, \quad (16)$$

and the interfacial unit normal vector is

$$n = -\frac{\nabla\rho^N}{\left|\nabla\rho^N\right|}. \quad (17)$$

The partial derivatives required for the curvature and normal vector calculations are obtained using the finite difference stencil

$$\partial_\alpha g = \frac{1}{c_s^2}\sum_i \omega_i g(x+e_i,t)e_{i\alpha}. \quad (18)$$

Using the recolouring step proposed by [Latva-Kokko and Rothman, 2005] to maintain the immiscibility of the fluids, the post-collision, recoloured red and blue fluid particle distribution functions are

$$r_i = \frac{\rho_R}{\rho}f_i + \beta\frac{\rho_R\rho_B}{\rho}\omega_i e_i\cdot n, \quad (19)$$

$$b_i = \frac{\rho_B}{\rho}f_i - \beta\frac{\rho_R\rho_B}{\rho}\omega_i e_i\cdot n, \quad (20)$$

where $\beta$ is a segregation parameter which is set to 0.7 for stability and model accuracy [Halliday *et al.*, 2007].

It should be noted that in regions where only one fluid is present, the interfacial force term and the recolouring step have no effect on the particle distribution functions, and the colour-fluid LB model then becomes the single phase lattice Boltzmann model.

## III. SIMULATION SETUP

In the simulations we use the D2Q9 discrete velocity model, where the discrete velocity $e_i$ and weight factor $\omega_i$ are

$$e_i = \begin{cases} (0,0) & i = 0 \\ (\pm 1, 0)c, (0, \pm 1)c & i = 1, 2, 3, 4 \\ (\pm 1, \pm 1)c & i = 5, 6, 7, 8 \end{cases}, \quad (21)$$

$$\omega_i = \begin{cases} 4/9 & i = 0 \\ 1/9 & i = 1, 2, 3, 4 \\ 1/36 & i = 5, 6, 7, 8 \end{cases}. \quad (22)$$

A parabolic velocity profile is enforced at the inlet channels and a fixed pressure boundary is enforced at the outlet channels [Zou, He, 1997]. At the microchannel walls we impose a no slip boundary using the midgrid bounceback scheme. We arbitrarily choose the droplet fluid to be the red fluid and the carrier fluid to be the blue fluid.

For each case, a T-junction upstream is used to generate droplets. The droplet fluid is introduced at the inlet normal to the downstream channel, and the carrier fluid is introduced at the inlet tangential to the downstream channel. Both inlet channels have the same width. The carrier fluid is set to have a greater wettability to the channel walls than the droplet fluid, which helps promote droplet breakup.

The simulations were carried out using our in-house LB code, which uses an indirect addressing scheme [Mattila *et al.*, 2008]. Compared to the direct addressing scheme, the indirect addressing scheme uses more memory per node and requires additional preprocessing steps. However, the indirect addressing scheme only requires fluid node information to be stored and does not require any solid node information to be retained. Therefore, when a significant proportion of solid nodes are present in the computational domain, the indirect addressing scheme is more memory efficient. In addition to this, boundary condition information at the walls is precalculated, eliminating the need for ghost nodes. For our 2D implementation, the indirect memory scheme is more memory efficient when less than 83% of the computational domain consists of fluid nodes, which is highly suitable for simulating complex geometries.

## IV. NUMERICAL RESULTS AND DISCUSSIONS

There are a number of dimensionless parameters which are important for characterising droplet generation. The capillary number

$$Ca = \frac{\eta_c u_c}{\sigma}, \quad (23)$$

where $\eta_c$ and $\mu_c$ are respectively the carrier fluid viscosity and velocity, is the ratio of viscous to interfacial forces that is the most important parameter. The flow rate ratio is

$$Q = \frac{Q_d}{Q_c}, \quad (24)$$

where $Q_d$ and $Q_c$ are the droplet and carrier phase flow rate respectively, and the viscosity ratio is

$$\lambda = \frac{\eta_d}{\eta_c}, \quad (25)$$

where $\eta_d$ is the droplet fluid viscosity. The Reynolds number

$$\mathrm{Re} = \frac{\rho_c u_c L_c}{\eta_c}, \quad (26)$$

where $L_c$ is the characteristic length, is the ratio of inertial to viscous forces and is also used to characterize droplet sizes (but has a much lesser effect than the other parameters). In our simulations, $Ca = 0.0125$, $\mathrm{Re} = 0.05$, $Q = 0.2$, $\lambda = 0.1$. This creates droplets that are large enough to occupy the full width of the microchannels and contribute to the fluidic resistance of the microchannel.

### IV.1. Case I

In this case we use the microchannel network shown in Fig. 1, based on the work of [Choi *et al.*, 2011], which has three different paths from the inlet to the outlet. We compare our LB results to the experimental work on bubble flows by [Choi *et al.*, 2011].

In the snapshot of Fig. 1, the droplets travel through each of the microchannel paths. From Fig. 2, which shows the velocity evolutionary behaviour at the centrelines of the two branches downstream of the first intersection for four droplet cycles, we find that the droplets will always enter the branch with the highest local velocity upon reaching an intersection. The additional fluidic resistance from the droplets travelling

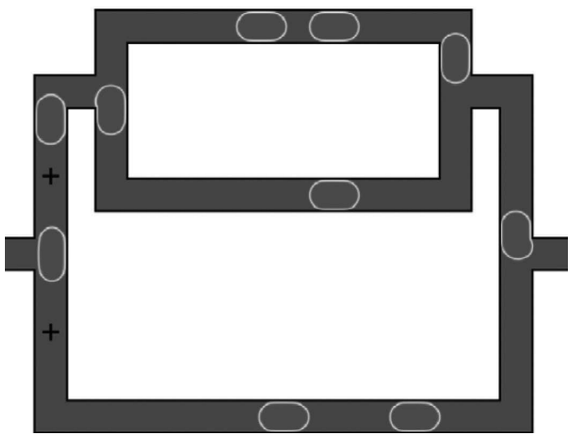


**Figure 1:** *Snapshot of Case I droplet simulation. The droplets flow from left to right. The black crosses indicate where velocity is measured.*

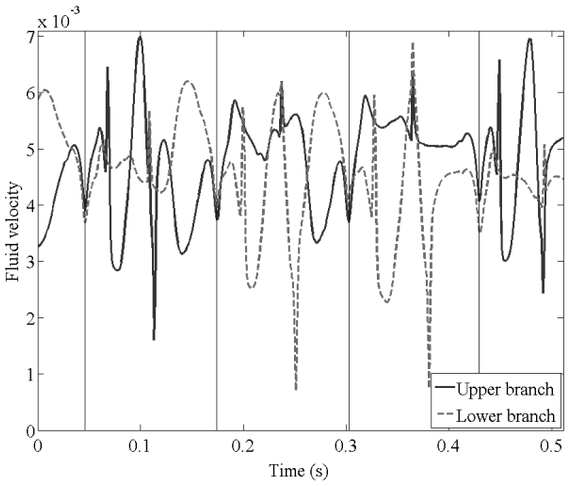


**Figure 2:** *Velocity evolutionary behaviour at the centrelines of the channel branches downstream of the first channel intersection (see Fig. 1) for Case I. A duration of four droplet periods is shown. The vertical black lines indicate the time step when the droplets begin to travel through one of the downstream branches. The first and fourth droplets travel through the upper branch. The second and third droplets travel through the lower branch.*

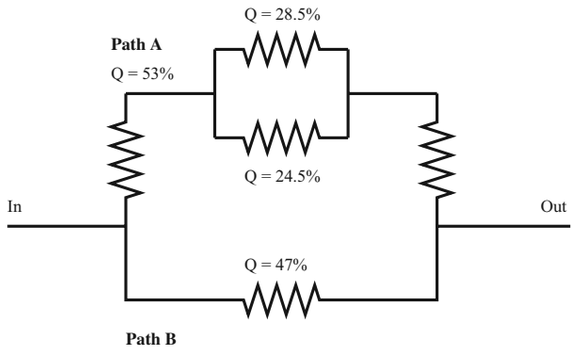


**Figure 3:** *Equivalent circuit of the microchannel network in Case I. Flow rates relative to the total channel flow rate are shown.*

through the microchannels would cause the microchannel flow rates to constantly fluctuate, which in turn would cause subsequent droplets to travel through different channel branches. This matches well with the experimental work by [Choi *et al.*, 2011], where, for an identical channel configuration, they observed similar bubble distribution behaviour and also found that bubbles would enter the branch with the highest local velocity.

We also investigate whether the proportion of droplets entering each microchannel branch can be predicted using single phase flow rates. The properties of a microfluidic network can in general be analysed using electrical circuit analysis techniques [Oh *et al.*, 2012]. Here, we compare hydraulic resistance properties of a microchannel network to electrical resistance in an electrical circuit, where the hydraulic resistance of a rectangular microchannel branch is approximately

$$R_H = \frac{12\eta L}{wh^3}, \tag{27}$$

where $L$ is the microchannel length, $w$ is the microchannel width and $h$ is the microchannel height. From equation (27) when the cross sectional area of a microchannel is fixed the channel resistance is approximately proportional to length. By treating individual microchannel segments as resistors and using electrical circuit theory, it is possible to determine the equivalent fluidic circuit for a microchannel network and therefore understand flow characteristics. Under single phase conditions, for the microchannel in Fig. 1, the equivalent fluidic circuit and the flow rates relative to the inlet flow rate is shown in Fig. 3. It can be seen that the flow rates of paths A and B are 53%, and 47% respectively. From the simulation results listed in Table 1, however, it can be clearly observed that a change in capillary number and flow rate ratio, which affects the droplet velocity and the number of droplets in the microchannel network at a given time, greatly changes the proportion of droplets travelling through each branch. We find that the single phase flow rates in a microchannel network does not bear any relation to the proportion of droplets travelling through each microchannel branch and therefore the single phase flow rates cannot be used to predict the proportion of droplets that will travel through each branch.

### IV.2. Case II

The microchannel network in Fig. 4 has two branches from the inlet to the outlet that are point symmetric around its centre. They have approximately the same fluidic resistance under single phase conditions and therefore have similar inlet velocities. Using this microchannel network, we further evaluate whether the previous observation, that droplets will travel along the downstream channel with the highest local velocity, holds true for a branch intersection where one of the downstream channel branches is tangential to the upstream channel.

Fig. 4 shows that the droplets travel through both microchannel branches, and we find that equal numbers of droplets enter each branch. In Fig. 5, which shows the velocity evolutionary behaviour at the two branches, we observe the same behaviour presented in Case I, where droplets, upon reaching an intersection, travel through the branch with the higher local velocity. This suggests that the highest local velocity rule may apply for arbitrary geometry.

### IV.3. Case III

The microchannel network shown in Fig. 6, also based on the work of [Choi *et al.*, 2011], is point symmetric around its centre. Although both microchannel branches should have very similar fluidic resistances under single phase conditions, the top channel has a much higher inlet velocity due to the width at the channel inlet being half the width of the bottom channel inlet. From the simulation snapshot in Fig. 6 it can be observed that all droplets entering the microchannel network travel exclusively through the upper channel branch. In Fig. 7, which shows the velocity evolutionary behaviour at the inlet of the channel branches, it can be seen that the upper channel branch, even with the additional fluidic resistance from the droplets within it, still has a significantly greater velocity than the lower channel branch. This effectively

*Table 1: Droplets entering the top (path A) and bottom (path B) branches (see Fig. 3) of the microchannel network in Case I.*

| Ca | Q | Droplets reaching intersection during simulation | Droplets travelling through Path A | Droplets travelling through Path B |
|---|---|---|---|---|
| 0.01 | 0.15 | 17 | 12 | 5 |
| | 0.2 | 22 | 12 | 10 |
| | 0.25 | 26 | 13 | 13 |
| | 0.3 | 30 | 16 | 14 |
| | 0.35 | 34 | 23 | 11 |
| 0.0125 | 0.15 | 22 | 15 | 7 |
| | 0.2 | 29 | 18 | 11 |
| | 0.25 | 34 | 16 | 18 |
| | 0.3 | 39 | 26 | 13 |
| | 0.35 | 44 | 39 | 5 |
| 0.015 | 0.15 | 27 | 14 | 13 |
| | 0.2 | 36 | 24 | 12 |
| | 0.25 | 42 | 23 | 19 |
| | 0.3 | 49 | 36 | 13 |
| | 0.35 | 55 | 42 | 13 |
| 0.0175 | 0.15 | 35 | 34 | 1 |
| | 0.2 | 43 | 26 | 17 |
| | 0.25 | 51 | 27 | 24 |
| | 0.3 | 59 | 48 | 11 |
| | 0.35 | 66 | 48 | 18 |

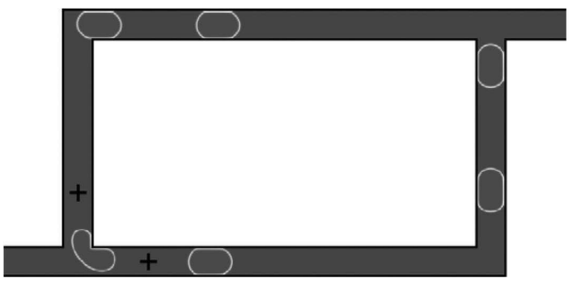

**Figure 4:** *Snapshot of Case II droplet simulation. The droplets flow from bottom-left to top-right. The black crosses indicate where velocity is measured.*

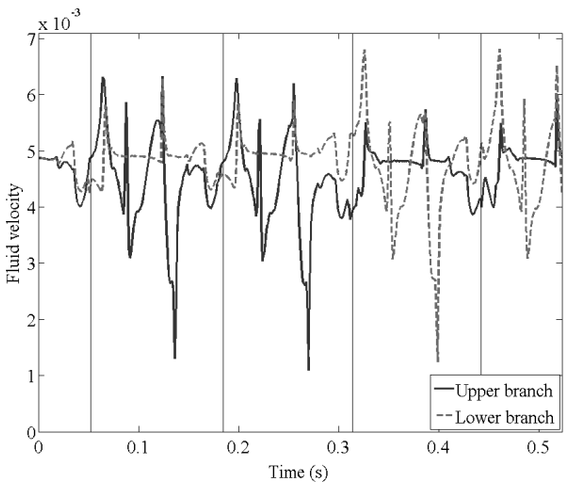


**Figure 5:** *Velocity evolutionary behaviour at the centrelines of the channel branches (see Fig. 4) for Case II. A duration of four droplet periods is shown. The vertical black lines indicate the time step when the droplets show signs of travelling through one of the downstream branches. The first two droplets travel through the upper branch. The other droplets travel through the lower branch.*

prevents any of the incoming droplets from travelling through the lower branch. A 3D simulation for this microchannel network was also carried out and the same results were obtained.

Research into microfluidic circuits has resulted in the development of many fluidic circuits with interesting behaviour, such as shift registers [Zagnoni, Cooper, 2010], flip flop gates [Prakash *et al.*, 2007], AND/OR and NOT gates [Cheo *et al.*, 2007]. We note that the flow of droplets in this microchannel geometry is similar to the flow of current in the electrical circuit shown in Fig. 8, where each branch effectively behaves like a resistor and diode connected in series and only permits the flow of droplets through one of the branches. For flows in the forward direction the droplets will travel through the top branch, while for flows in the reverse direction the droplets will travel through the bottom branch.

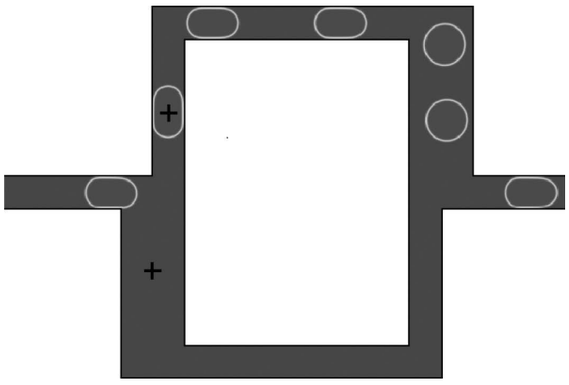

**Figure 6:** *Snapshot of Case III droplet simulation. The droplets flow from left to right. The black crosses indicate where velocity is measured.*

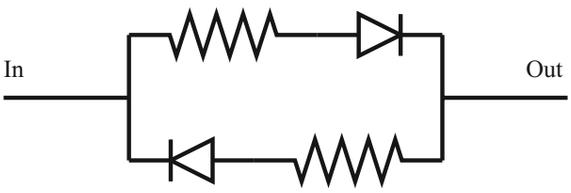


**Figure 8:** *Equivalent electric circuit which shows similar behaviour to the microchannel network in Case III. If a DC voltage is applied, current will only pass through one of the two branches.*

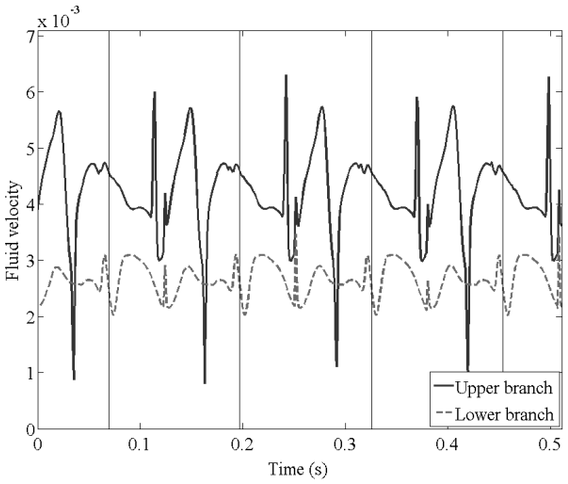


**Figure 7:** *Velocity evolutionary behaviour at the centrelines of the channel branches near the inlets (see Fig. 6) for Case III. A duration of four droplet periods is shown. The vertical black lines indicate the time step when the droplets begin to travel through one of the downstream branches. All the droplets travel through the upper channel branch.*

## V. CONCLUSIONS

Multiphase lattice Boltzmann simulations have been carried out to study droplet flow in three different microchannel networks. The lattice Boltzmann method was shown to be suitable for simulating microdroplet flows in complex microchannel networks. We found that droplets that are large enough to occupy the full width of a microchannel, upon reaching a channel intersection, will travel through the downstream branch with the highest local velocity. Our results suggest that this may apply to arbitrary geometry. We also revealed that single phase flow rates cannot be used to predict the proportion of droplets travelling through the individual branches of a microchannel network.

## VI. REFERENCES

Brackbill J. U., Kothe D. B., Zemach C. (1992) — A Continuum Method for Modeling Surface Tension. *J. Comp. Phys.* **100** : 335-354

Chen S., Doolen G. D. (1998) — Lattice Boltzmann method for fluid flows. *Annu. Rev. Fluid Mech.* **30** : 329-64

Cheow L. F., Yobas L., Kwong D. L. (2007) — Digital Microfluidics : Droplet based logic gates. *Appl. Phys. Lett.* **90** : 054107

Christopher G. F., Noharuddin N. N., Taylor J. A., Anna S. L. (2008) — Experimental observations of the squeezing-to-dripping transition in T-shaped microfluidic junctions. *Phys. Rev. E.* **78** : 036317

Choi W., Hashimoto M., Ellerbee A. M., Chen X., Bishop K. J. M., Garstecki P., Stone H. A., Whitesides G. M. (2011) — Bubbles navigating through network of microchannels. *Lab Chip.* **11** : 3970 - 3978

Garstecki P., Fuerstman M. J., Stone H. A., Whitesides G. M. (2006) — Formation of droplets and bubbles in a microfluidic T-junction - scaling and mechanism of break-up. *Lab Chip.* **6** : 437-446

Glawdel T., Elbuken C., Ren C. (2011) — Passive droplet trafficking at microfluidic junctions under geometric and flow asymmetries. *Lab Chip.* **11** : 3774-3784

Gunstensen A. K., Rothman D. H., Zaleski S., Zanetti G. (1991) — Lattice Boltzmann model of immiscible fluids. *Phys. Rev. A.* **43(8)** : 4320

Gupta A., Kumar R. (2010) — Flow regime transition at high capillary numbers in a microfluidic T-junction : Viscosity contrast and geometry effect. *Phys. Fluids.* **22** : 122001

Halliday I., Hollis A. P., Care C. M. (2007) — Lattice Boltzmann algorithm for continuum multicomponent flow. *Phys. Rev. E.* **76** : 026708

Latva-Kokko M., Rothman D. H. (2005) — Diffusion properties of gradient-based lattice Boltzmann models of immiscible fluids. *Phys. Rev. E.* **71** : 056702

Lishchuk S. V., Care C. M., Halliday I. (2003) — Lattice Boltzmann algorithm for surface tension with greatly reduced microcurrents. *Phys. Rev. E.* **67** : 036701

Liu H., Zhang Y. (2011) — Droplet formation in microfluidic cross-junctions. *Phys. Fluids.* **23** : 082101

Mattila K., Hyväluoma J., Timonen J., Rossi T. (2008) — Comparisons of implementations of the lattice-Boltzmann method. *Computers Math. Applic.* **55** : 1514-1524

Mohr S., Zhang, Y, Macaskill A., Day P. J. R., Barber R. W., Goddard N. J., Emerson D. R., Fielden P. R. (2007) — Numerical and experimental study of a droplet-based PCR chip. *Microfluid. Nanofluid.* **3** : 611-621

Oh K. W., Lee K., Ahn B., Furlani E. P. (2012) — Design of pressure-driven microfluidic networks using electric circuit analogy. *Lab Chip.* **12** : 515-545

Parthiban P., Khan S. A. (2012) — Filtering microfluidic bubble trains at a symmetric junction. *Lab Chip*. **12** : 582-588

Prakash M., Gershenfeld N. (2007) — Microfluidic bubble logic. *Science*. **315** : 832-835

Qian Y. H., D'humieres D., Lallemand P. (1992) — Lattice BGK Models for Navier-Stokes Equation. *Europhys. Lett.* **17(6)** : 479-484

Stone H. A., Stroock A. D., Ajdari A. (2004) — Engineering Flows in Small Devices : Microfluidics towards a Lab-on-a-Chip. *Annu. Rev. Fluid Mech.* **36** : 381-411

Van Der Graaf S., Nisisako T., Schron C. G. P. H., Van Der Sman R. G. M. Boom R. M. (2006) — Lattice Boltzmann Simulations of Droplet Formation in a T-Shaped Microchannel. *Langmuir.* **22(6)** : 4144-4152

Xu J. H., Luo G. S., Li S. W., Chen G. G. (2006) — Shear force induced monodisperse droplet formation in a microfluidic device by controlling wetting properties. *Lab Chip.* **6** : 131-136

Zagnoni M., Cooper J. M. (2010) — A microdroplet-based shift register. *Lab Chip.* **6** : 3069-3073

Zou Q., He X. (1997) — On pressure and boundary conditions for the lattice Boltzmann BGK model. *Phys. Fluids.* **9(6)** : 1591-1598